Seismic Behavior and Fragility Curves of Replaceable Steel Coupling Beams with Slabs

Xiaodong Ji[a], Yandong Wang[a], Junshan Zhang[a], Taichiro Okazaki[b]

[a]Key Laboratory of Civil Engineering Safety and Durability of China Education Ministry, Department of Civil Engineering, Tsinghua University, Beijing 100084, China

[b]Graduate School of Engineering, Hokkaido University, Sapporo, Hokkaido 060-8628, Japan

Abstract: Replaceable steel coupling beams (RSCB) have been proposed as an alternative to conventional reinforced concrete (RC) coupling beams for enhanced seismic resiliency of coupled wall systems. This paper presents a series of quasi-static tests conducted to examine the seismic behavior of RSCBs with RC slabs and to identify reasonable slab configurations that can minimize the damage to RC slabs. A total of five large-scale specimens were designed and tested. The first four specimens adopted the same end plate link-to-beam connection but adopted different types of RC slabs, including a composite slab, bearing slab, isolated slab or slotted slab. The fifth specimen adopted splice plate link-to-beam connection and a bearing slab. The test results indicate that all specimens developed a large inelastic rotation capacity of more than 0.05 rad with stable hysteretic response. The presence of RC slabs is found to have limited effect on the shear strength and inelastic rotation capacity of RSCBs. Some types of RC slabs increased the initial elastic stiffness of RSCBs, but in the plastic stage, none of the slabs affected the loading or unloading stiffness. Among those four types of slabs, the composite slab suffered the most significant damage, as a result of pulling out of shear studs and subsequent pouching failure of the slab. Compared with the bearing

Please cite this article as: Xiaodong Ji, Yandong Wang, Junshan Zhang, Taichiro Okazaki. Seismic behavior and fragility curves of replaceable steel coupling beams with slabs. Engineering Structures, 2017, 150(1): 622-635. doi: 10.1016/j.engstruct.2017.07.045

slab or slotted slab, the isolated slab developed much fewer and smaller cracks, which should allow for easier repair. Based on the observations of this test and previous tests, four damage states for RSCBs were identified, corresponding to different repair methods. Fragility curves of RSCBs at various damage states were developed, which can provide the criteria for seismic performance assessment of RSCBs.

Keywords: replaceable steel coupling beam; RC slab; cyclic behavior; slab damage; crack; fragility curve.

1. Introduction

Coupled wall systems are often used in high-rise buildings due to their superior strength and stiffness against wind load and earthquake action. Coupling beams distributed along the building height are designed as the components that undergo inelastic deformation and dissipate energy when the coupled wall systems are subjected to strong seismic motions. If detailed appropriately, reinforced concrete (RC) coupling beams show adequate seismic performance, but once damaged, post-earthquake repair of these components requires significant cost in expense and time. For enhanced seismic resiliency for buildings, there is a clear need to develop innovative coupling beams that are easy to repair or replace after being damaged. Recently, various types of replaceable coupling beams have been proposed and recognized as an alternative to RC coupling beams [1,2,3,4,5].

Figure 1 shows a type of replaceable steel coupling beam (RSCB), which comprises a central "fuse" shear link connected to steel beam segments at its two ends. By appropriately proportioning the strengths of beam segments and the shear links, inelastic deformation and damage are expected to concentrate in the "fuse" shear links when the coupled wall is subjected to severe ground motion. Past studies (e.g., Kasai and Popov [6], Dusicka et al. [7], Ji et al. [8]) indicate that short shear link with proper detailing can provide large inelastic deformation, stable hysteretic responses and significant energy dissipation. In addition, specialized link-to-beam connections have been developed which can ensure adequate shear and flexural strength of the connections and allow the damaged shear link to be replaced easily in presence of residual drifts [4]. Large-scale tests by Ji et al. [4] have demonstrated the excellent seismic performance and replaceability of the RSCBs. Nevertheless, the previous tests were on bare RSCBs, and they did not include the slabs above the coupling beams. The presence of RC slabs might influence the strength and deformation capacity of the beneath RSCBs. Moreover, RC slabs possibly suffer severe damage at large inelastic rotation of the RSCBs, which would influence the post-quake recovery of buildings.

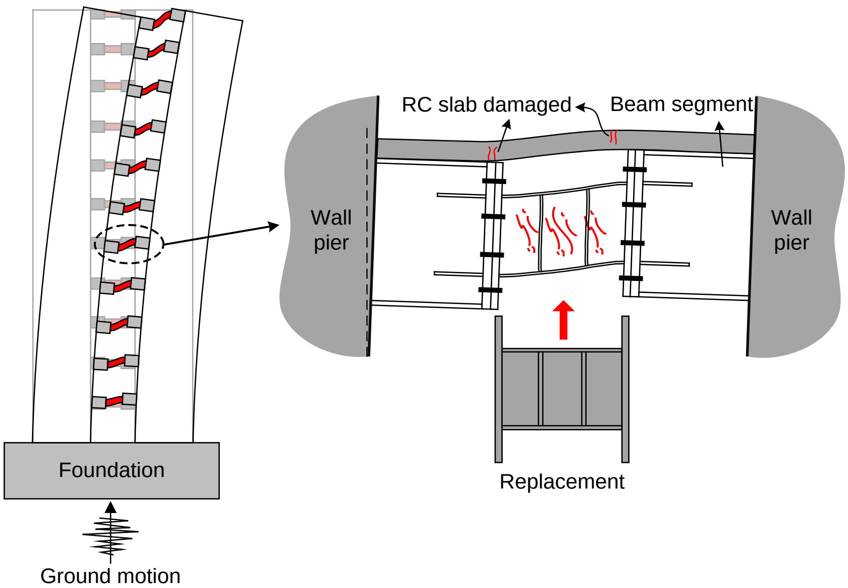

Fig. 1. Replaceable steel coupling beam with RC slab

To this end, the objectives of this paper are to examine how the seismic behavior of RSCBs is affected by the presence of RC slabs and to identify reasonable slab configurations for RSCBs that can minimize slab damage. This paper presents four types of RC slabs, i.e., composite slab, bearing slab, isolated slab and slotted slab. Large-scale specimens of RSCBs with different types of RC slabs were tested under cyclic loading. The next section presents the specimen design and experimental program. The third section details the test results, including hysteretic responses and damage to the RSCBs and above RC slabs. The fourth section examines the influence of RC slabs on the stiffness, strength and inelastic rotation capacity of RSCBs. Finally, based on the results in this test program and past tests, the fifth section develops fragility functions for RSCBs with RC slabs which provide the criteria for seismic performance assessment of RSCBs.

2. Experimental program

2.1. Test specimens

2.1.1. Replaceable steel coupling beams

Ji et al. [4] have reported cyclic shear tests of four bare RSCBs representative of 5/6-scale prototype coupling beams adopted in an eleven-story building. Except for addition of RC slabs, the specimens in this paper were identical in scale and dimension to the bare RSCB specimens in previous tests. Figure 2 shows the geometry and details of the specimens. Two types of link-to-beam connections were adopted, i.e. end plate connection for Specimen CBS1 through CBS4 and splice plate connection for Specimen CBS5. For the end plate connection, the shear key set in the end plate was used to transfer all shear force and the high-strength bolts were designed to resist the bending moment. For the splice plate connection, the flange splices were designed to resist all the moment at the centerline of the splice and the web splices were design to resist all shear force acting at the centerline of the splice. Ji et al. [4] reported that these two types of specialized link-to-beam connections can ensure excellent seismic performance of RSCBs and allow easy replacement of damaged links.

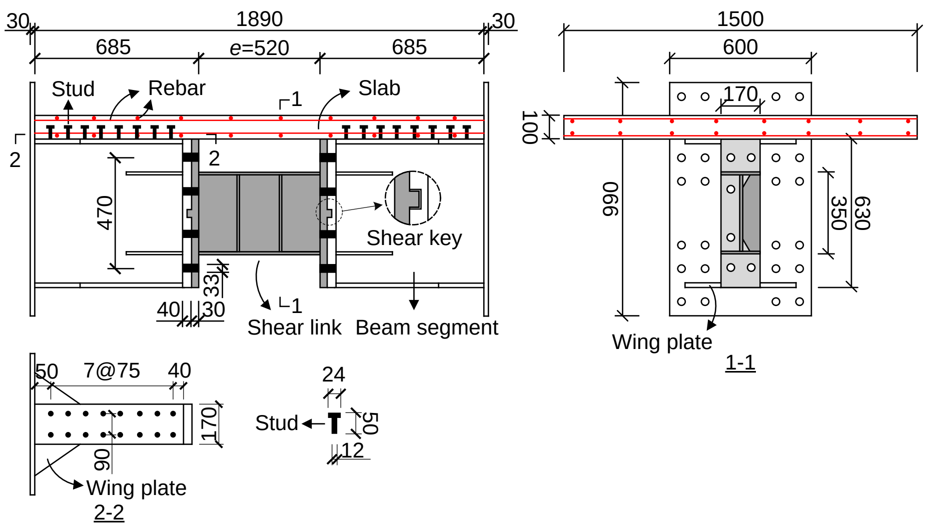

(a) CBS1 (composite slab)

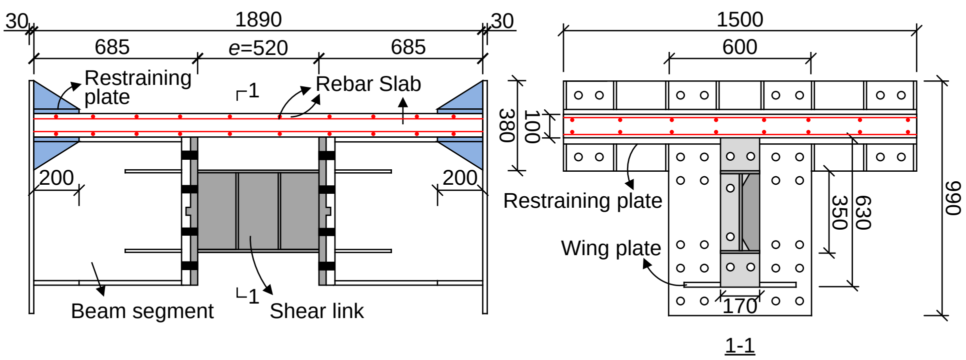

(b) CBS2 (bearing slab)

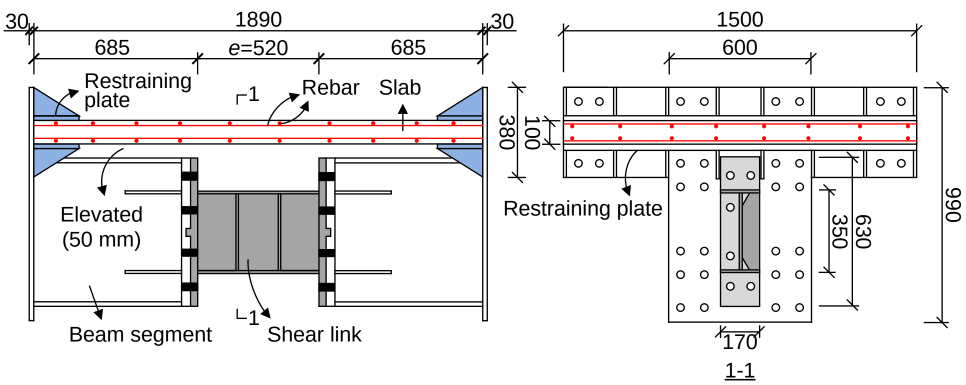

(c) CBS3 (isolated slab)

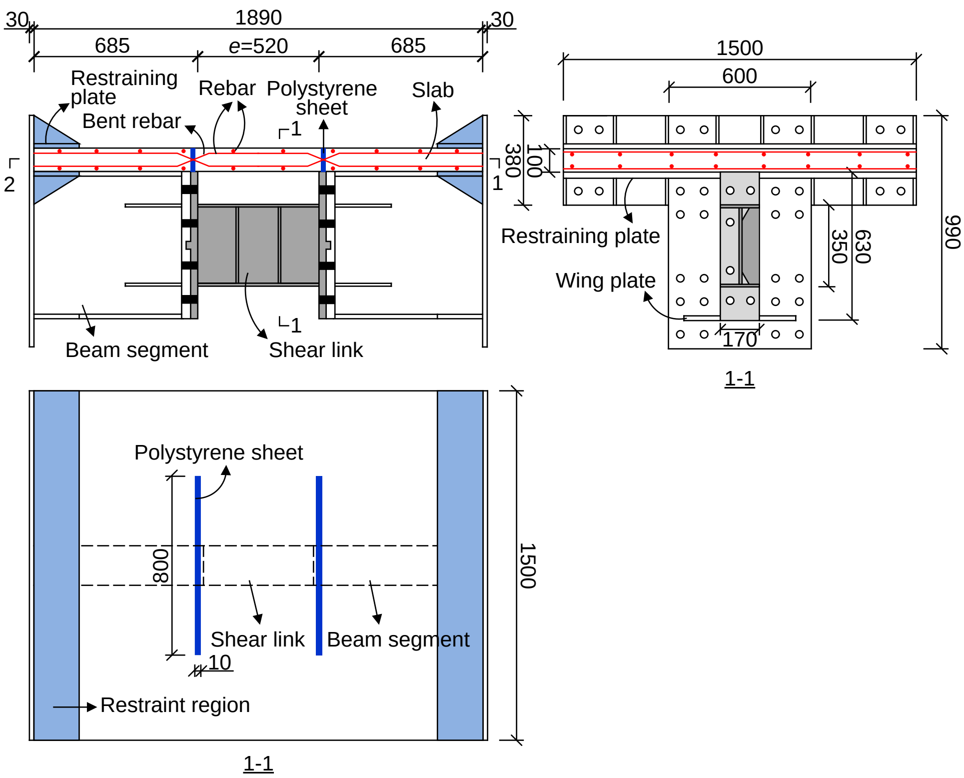

(d) CBS4 (slotted slab)

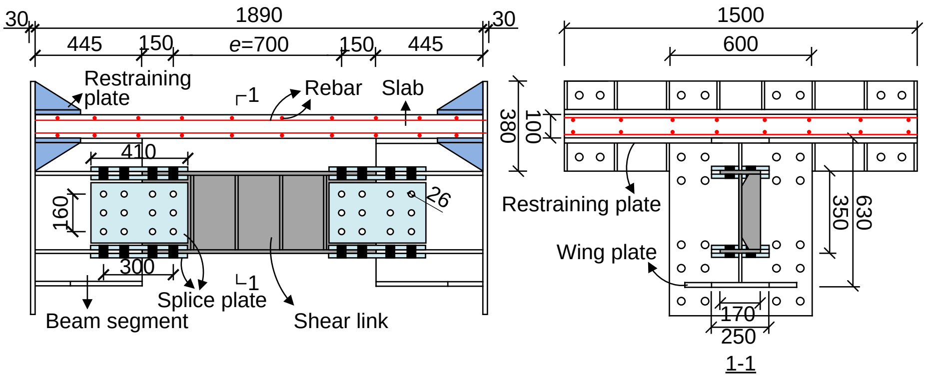

(e) CBS5 (bearing slab)

Fig. 2. Test specimens

Table 1 summarizes design parameters of the specimens. The shear links were built-up sections of H 350 × 170 × 10 × 12 (depth × flange width × web thickness × flange thickness, unit: mm) for Specimens CBS1 through CBS4 and H 350 × 170 × 10 × 16 for Specimen CBS5. The link flanges and web were welded by complete-joint-penetration (CJP) groove welds. Hybrid sections with lower yielding strength steel in web are used for the shear links to promote early yielding in shear and to increase their inelastic rotation capacity. The link web was low-yield-strength steel LY225 (nominal yield strength f_y = 225 MPa), the link flanges were Q345 steel (f_y = 345 MPa), and the stiffeners were Q235 steel (f_y = 235 MPa). Table 2 lists the material properties determined based on tensile coupon tests. Both the link flange and web satisfied the compactness requirement for highly ductile shear links by the AISC 341-10 provisions [9].

Table 1. Design parameters of specimens

Spec. No.	Slab type	Link-to-beam connection	Shear link				Beam segment
			Section	Length ratio $e/(M_p/V_p)$	Flange compactness $b_f/(2t_f)$	Web compactness h_0/t_w	Section
CBS1	Composite	End plate connection	H350×170 ×10×12	0.70	7.1	32.6	H630×170 ×16×20
CBS2	Bearing						
CBS3	Isolated						
CBS4	Slotted						
CBS5	Bearing	Splice plate connection	H350×170 ×10×16	0.76	5.3	31.8	H630×250 ×16×20

Note: e denotes the link length (Fig. 2), and M_p and V_p denote the plastic flexural strength and shear strength of link, respectively.

Table 2. Material properties for steel of shear links

Steel type	Plate	Thickness t (mm)	Yield strength f_y (MPa)	Ultimate strength f_u (MPa)	f_y/f_u	Elongation δ (%)
LY225	Web	10	235	318	0.74	47
Q235	Stiffener	10	288	406	0.71	43
Q345	Flange of CBS1, CBS2, CBS3, CBS4	12	357	521	0.69	43
Q345	Flange of CBS5	16	347	519	0.67	46

All links had a length ratio, $e/(M_p/V_p)$, smaller than 1.6 and, therefore, they were expected to yield primarily in shear. The stiffeners of shear link were full depth, welded to the link web and to both link flanges using fillet welds, and placed on one side of the web only.

The stiffener spacing satisfied the limit for shear links specified by AISC 341-10 [9]. To delay web fracture at the region where the flange-to-web CJP groove weld and the stiffener-to-web fillet welds meet, the vertical fillet welds were terminated at a distance of no less than five times the web thickness from the flange-to-web weld [10,11].

To ensure that the beam segments remain elastic when the shear link fully yields and strain-hardens, their strength was designed to exceed the strength demand corresponding to the overstrength of shear link. Considering the very small length ratio of approximately 0.7, the overstrength factor of shear links was taken as 1.9 as suggested by Ji et al. [8]. Similarly, the strength of link-to-beam connection was designed to exceed the overstrength capacity of shear links. The details of link-to-beam connection design can be found in Reference [4].

2.1.2. RC slab design

The slabs of all specimens had identical dimensions and reinforcement, as shown in Fig. 3. The slab width was 1500 mm, much larger than the effective flange width of composite beams which is 630 mm based on Chinese Code for Design of Concrete Structures (GB 50010-2010) [12]. The slab thickness was 100 mm, i.e., 5/6 scale of the prototype slab thickness of 120 mm. The reinforcement of slabs were designed in accordance with the GB 50010-2010 provisions [12]. D8 (diameter = 8 mm) rebar meshes were placed in two layers, with the spacing of rebars no greater than 200 mm in both directions.

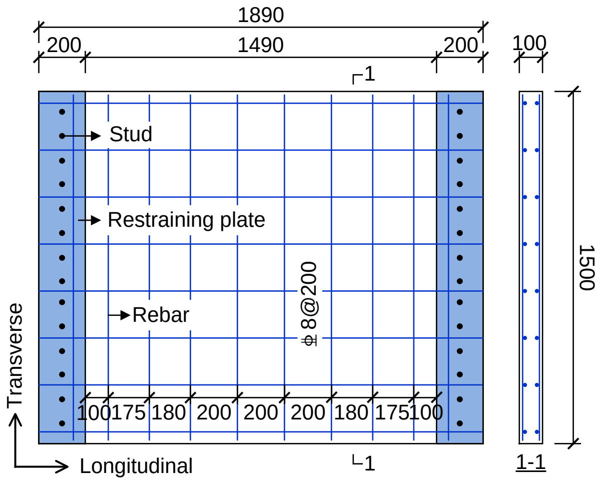

Fig. 3. Dimensions and reinforcement of RC slab

The strength grade of the slab concrete in all specimens was C30 (the nominal cubic compressive strength f_{cu} = 30 MPa, and the design value of axial compressive strength f_c = 14.3 MPa). The cubic strength of the concrete $f_{cu,t}$ measured at the time of specimen testing was 28.8 MPa, represented by the average strength tested on three cubes of 150 mm size. The strength grade of rebars was HRB400 (nominal yield strength f_y = 400MPa). The measured yield strength f_y by tensile coupon tests was 378 MPa and the measured ultimate tensile strength f_u was 658 MPa.

2.1.3. Slab configurations

To minimize the damage to RC slabs above RSCBs, various types of slab configurations are proposed and designed for comparison.

(1) Composite slab

In Specimen CBS1, headed studs were used achieve composite action between the steel beam segments and RC slabs. The partially composite beam was designed with the number of shear studs equal to half of the minimum required to achieve fully composite action. No shear studs were placed on the links because the shear link is recognized as a protected zone and because the link was placed 180 mm below the RC slab. The headed studs were 50 mm in length and

12 mm in diameter, and their location as shown in Fig. 2(a).

(2) Bearing slab

Ricles and Popov [13] reported a series of comparative experiments on bare eccentrically braced frames (EBFs) and EBFs with composite deck slabs. Much of the slab damage occurred in the proximity to the link, where transverse cracks occurred and shear studs were pulled out from the slabs. Mansour et al. [14] reported similar damage pattern for the composite deck slabs of EBFs. To prevent the pulling out of shear studs and related damage in RC slabs, Specimen CBS2 and CBS5 did not use shear studs, as shown in Fig. 2(b) and (e). The RC slab was cast on the RSCBs without shear connectors.

(3) Isolated slab

Under large rotation of RSCBs, the steel beam segment may bear the above RC slabs, which would result in kinking deformation and unwanted damage of RC slabs. Therefore, in Specimen CBS3 (see Fig. 2(c)), the RC slab was elevated by 50 mm from the top flanges of beam segments, which ensured that RC slab and beam segments did not contact each other even at 0.06 rad coupling beam rotation.

(4) Slotted slab

Castiglioni et al. [15] proposed a slotted slab configuration, where gaps perpendicular to the beam were set in the RC slab above the fuses, and found this configuration to be effective in limiting damage to RC slabs. Specimen CBS4 adopted the configuration of slotted slab, where two 800 mm slots were realized by placing polystyrene sheets in the slab above the link-to-beam connections. The slot width of 10 mm was chosen to avoid contact of concrete divided by the slot during cyclic loading. The slots extended beyond the effective width of composite slabs, but the slots did not completely separate the slab which is intended to retain the slab's ability to serve as a rigid diagram and transfer initial forces. The longitudinal rebars were bent at the slots to form a pinned connection, as shown in Fig. 2(d).

2.2. Test setup, instrumentation and loading protocol

Figure 4 shows the test setup. All specimens were securely clamped to two steel frame columns. These frame columns were designed with large stiffness to simulate the restraint provided by wall piers. The columns were pinned to the foundation beam at one end and pinned to the rigid loading beam at the other end.

For Specimen CBS1, the composite slabs were unrestrained at the ends except at the end plates where the longitudinal rebars were welded to the beam end plates and the slab could bear against the end plate. For the remaining four specimens, the RC slabs were restrained at the ends. As shown in Fig. 4, the beam end plate was extended to the full width of slab at the slab height, and was backed up by two auxiliary beams. Two restraining plates were rigidly connected to the beam end plates with stiffeners. The slab was clamped by the restraining plates and the longitudinal rebars were plug welded to the beam end plates. Such boundary conditions provided flexural, axial and shear restraints to the RC slab in one direction, which simulated the restraints to the prototype slab provided by the shear walls and adjacent slabs. It is noted that the prototype slab is supported in two sides and has restraints in two directions in the building, which provides more complicated boundary conditions than the slab in this test. However, accurate simulation for such boundary conditions requires a very substantial testing setup, which is left for future study.

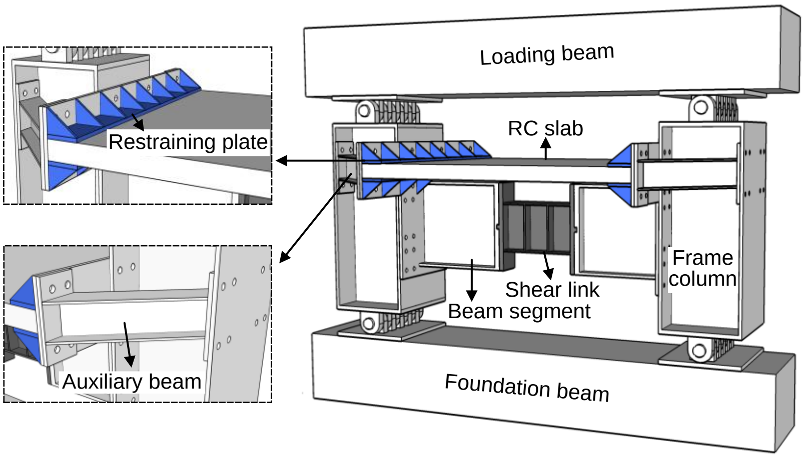

Fig. 4. Illustration of test setup

Instrumentation was used to measure load, displacements and strains at the locations shown in Fig. 5. The shear force of the coupling beam specimen was calculated based on moment equilibrium and using the data of lateral load measured by a load cell. Chord rotation of the coupling beam (referred to as "beam rotation" hereinafter) was measured by crossed linear variable differential transformers (LVDTs) D1 and D2, while rotation of the shear link (referred as "link rotation") was measured by crossed LVDTs D3 and D4. Strain gauges measured the strains in shear links, beam segments and longitudinal rebars of RC slabs.

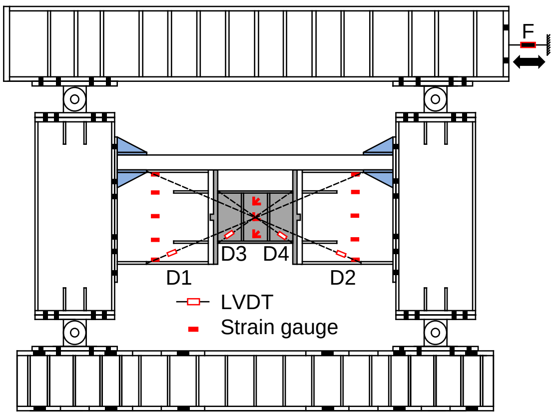

(a) Instrumentation of RSCB

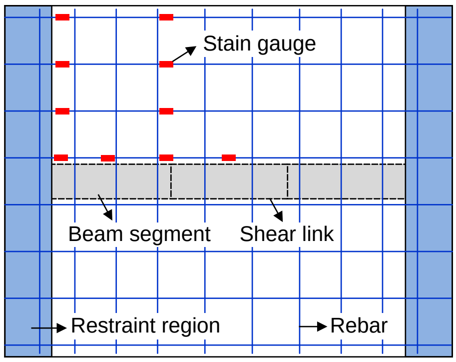

(b) Instrmentation of reinforcements

Fig. 5. Instrumentation of specimens

Figure 6 shows the loading protocol of the test. Cyclic loading was force-controlled before the yielding of shear link, and two levels of shear forces (i.e., $0.5V_p$ and V_p) were considered. The yielding strength of the specimen was estimated as the plastic shear strength of the link $V_p = 0.6f_yA_w$, where f_y denotes the measured yield strength of link web steel and A_w denotes the cross-sectional area of link web. Note that this estimation neglects the shear strength contribution of RC slab. Simplified calculation indicates the shear force provided by the RC slab is limited, which is corroborated by the test results described later in Section 4. After yielding of shear link, the loading was changed to displacement control. The beam rotation increased in increments of 0.005 rad before 0.02 rad and then increased in increments of 0.01 rad. Two cycles were repeated at each loading level. The test for Specimens CBS2 through CBS4 was terminated when these specimens significantly lost their shear strength. The loading of Specimens CBS1 and CBS5 was terminated after 0.06 rad beam rotation as the lateral displacement was close to the capacity of the loading facility, although they did not exhibit significant strength decrease.

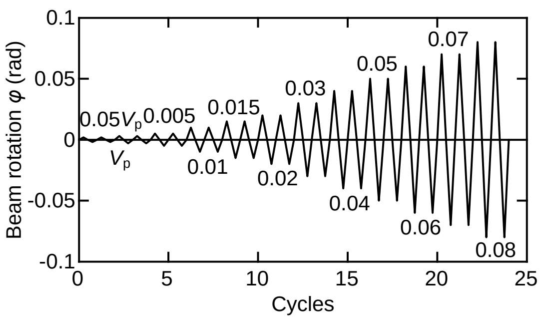

Fig. 6. Loading protocol

3. Experimental results

3.1. Hysteretic response

Figure 7 shows the hysteresis curves of shear force versus beam rotation for each specimen. Specimens with end plate link-to-beam connection showed stable hysteretic behavior under large inelastic rotation. The beam segment of Specimen CBS3 failed at 0.05 rad beam rotation due to fracture of the welds between beam flange and beam end plate. It is suspected that this failure, which was not expected, was caused by weld defects. Specimen CBS5, with splice plate link-to-beam connection, exhibited "pinching" in hysteretic loops due to slippage of high-strength bolts, which was discussed in Ji et al. [4].

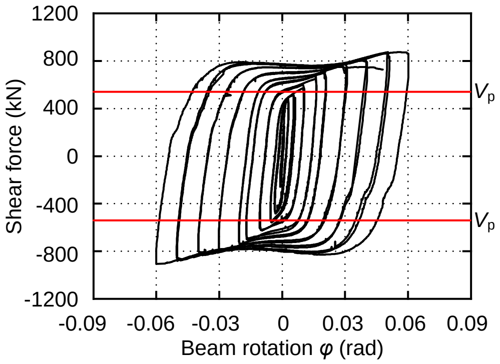

(a) CBS1

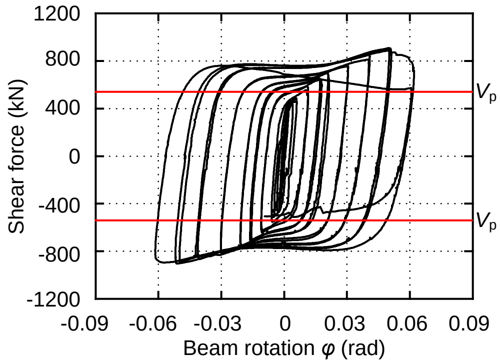

(b) CBS2

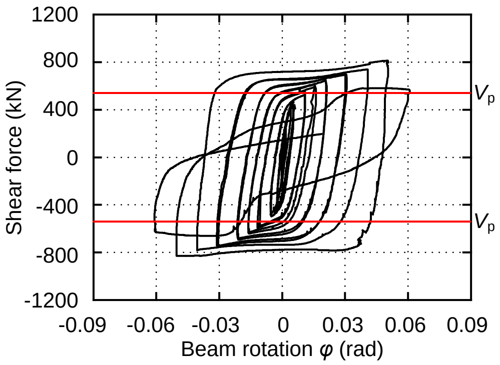

(c) CBS3

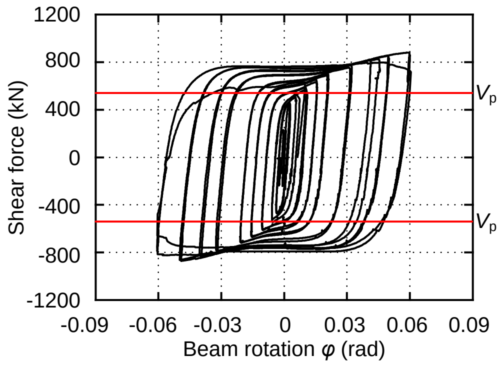

(d) CBS4

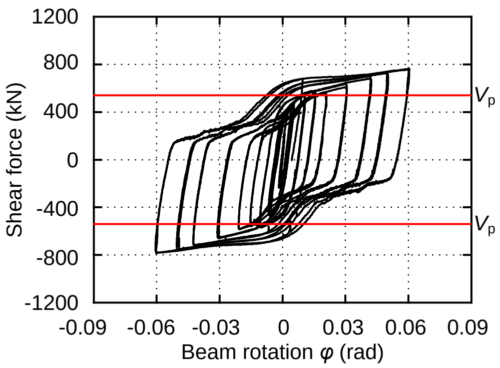

(e) CBS5

Fig. 7. Hysteretic responses of specimens

3.2. Damage to shear links

Table 3 summarizes the progression of visually identified damages of shear links and the cause of ultimate failure. In this paper, failure of the specimen is defined as the point where the shear strength drops to below the link plastic strength V_p.

Table 3. Damage and failure process of shear links

Spec. No.	Rotation of coupling beam (shear link) at damage occurrence (rad)					Failure mode
	Shear link damage					
	Web buckling	Global buckling	Stiffener-to-web weld fracture	Flange-to-end plate weld fracture	Flange local buckling	
CBS1	0.04 (0.12)	—	0.04 (0.12)	0.06 (0.18)	0.06 (0.18)	Flange-to-end plate weld fracture
CBS2	—	—	0.04 (0.12)	0.06 (0.18)	0.06 (0.18)	Flange-to-end plate weld fracture
CBS3	—	0.04 (0.12)	0.04 (0.12)	—	—	—
CBS4	—	0.05 (0.15)	0.04 (0.13)	0.06 (0.17)	0.06 (0.17)	Flange-to-end plate weld fracture
CBS5	—	—	—	—	—	—

Web buckling, web fracture and flange-to-end plate weld fracture were observed in shear links, which are consistent with past experiments [4,8,10,16]. Global and flange local buckling was also observed in shear links, as shown in Fig. 8, although buckling deformation did not appear to cause failure. Note that both local and global buckling was plastic buckling, which occurred later than the yielding of links. As discussed by Ji et al. [4], axial restraint by the frame columns, which simulates the axial restraint of wall piers to coupling beams, gives rise to substantial axial forces at large rotation cycles, which leads to plastic elongation, which, in turn, exacerbates compression. The large compression causes the pinching of the hysteresis curve near zero rotation. In fact, global link buckling was observed in Specimens CBS3 and CBS4, all of which exhibited pinching as shown in Fig. 7. In Specimen CBS1, CBS2 and CBS4, the force redistribution following fracture of a tension flange appeared to trigger local buckling of the compression flange at the same end.

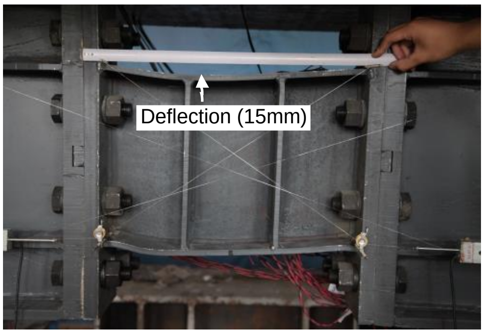

(a) Global buckling

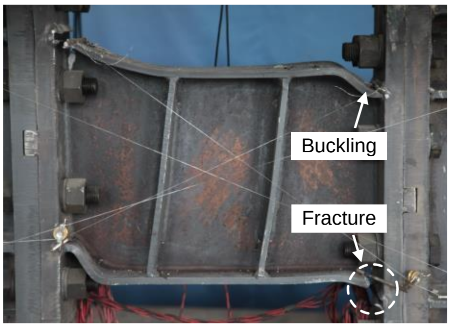

(b) Flange-end plate weld fracture and flange local buckling

Fig. 8. Photographs of link damage

The shear link of Specimen CBS1, CBS2 and CBS4 failed by the flange-to-end plate weld fracture at 0.06 rad beam rotation. Fracture was not observed in the shear link of Specimen CBS3. For Specimens CBS5, bolt slippage was clearly observed beyond 0.015 rad beam rotation cycles. Compared to specimens that adopted the end plate link-to-beam connection, link damage in Specimen CBS5 was mild, likely because a significant part of inelastic rotation was absorbed by bolt slippage.

3.3. Damage to RC slabs

Figure 9 shows photographs of damage to the RC slab of each specimen. Concrete cracking, which was observed commonly in all specimens, will be discussed later. For Specimen CBS1, the composite slab began to separate from the beam segment at 0.005 rad beam rotation. At 0.04 rad beam rotation, almost all the shear studs were pulled out from the RC slab, the concrete slab sustained punching failure, and rebars were exposed and buckled, as shown in Fig 9(a). For Specimens CBS2 and CBS5 with bearing slabs, slight concrete crushing was observed on the bottom surface of the slabs in the region where the beam segments bore against the slab. For Specimen CBS3 with isolated slab, concrete crushing was not observed. For Specimen CBS4, concrete spalling occurred on the bottom surface in the vicinity of slots.

It is notable that for all specimens, slight concrete crushing was observed near the restraint regions at the ends. This local damage was strongly affected by the boundary condition facilitated by the test.

(a) CBS1 (composite slab)

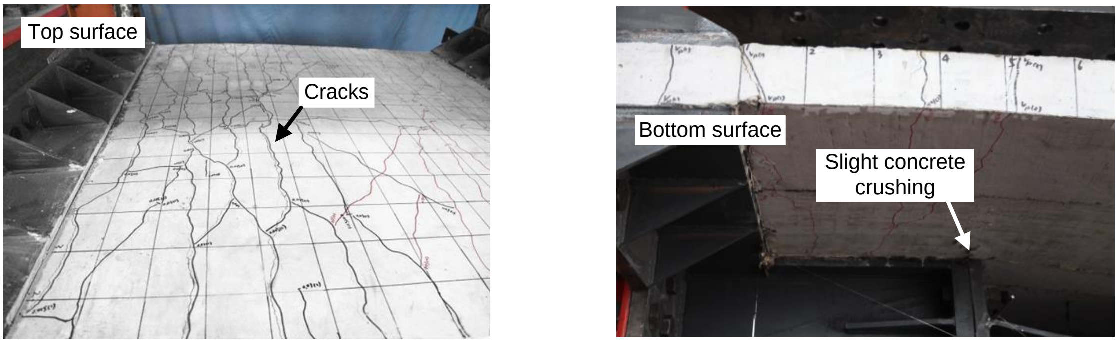

(b) CBS2 (bearing slab)

(c) CBS3 (isolated slab)

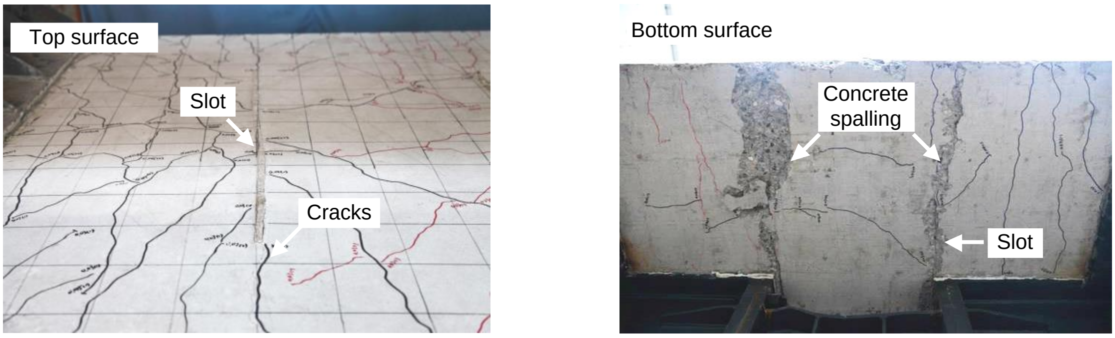

(d) CBS4 (slotted slab)

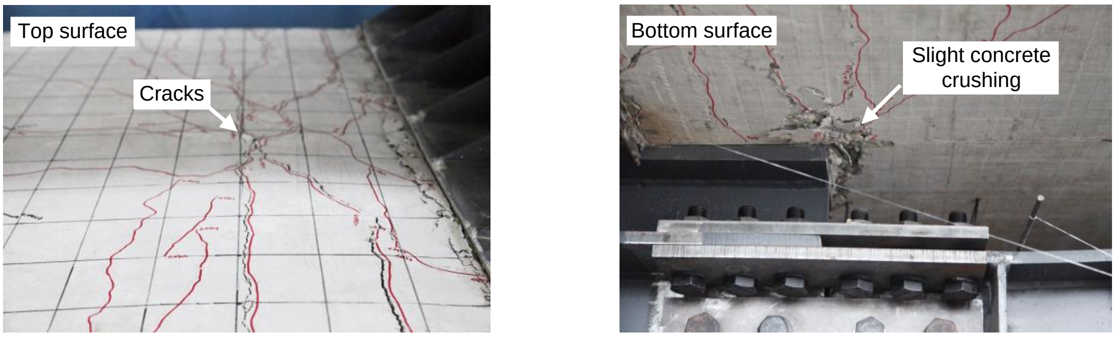

(e) CBS5 (bearing slab)

Fig. 9. Photographs of RC slab damage

3.3.1. Cracking patterns

Figure 10 shows the cracks that occurred on the top surface of slabs. The initial transverse cracks were observed at 0.003 to 0.005 rad beam rotation. Cracks were fully developed at 0.03 rad beam rotation, and very limited number of new cracks occurred afterwards.

The isolated slab had a few cracks, and those few cracks formed in the transverse direction and only near the ends. The other types of slabs developed much denser transverse cracks than the isolated slab, and developed longitudinal and diagonal cracks which were not seen in the isolated slab. The cracking patterns are similar to those reported by Mansour et al. [14] for composite deck slabs.

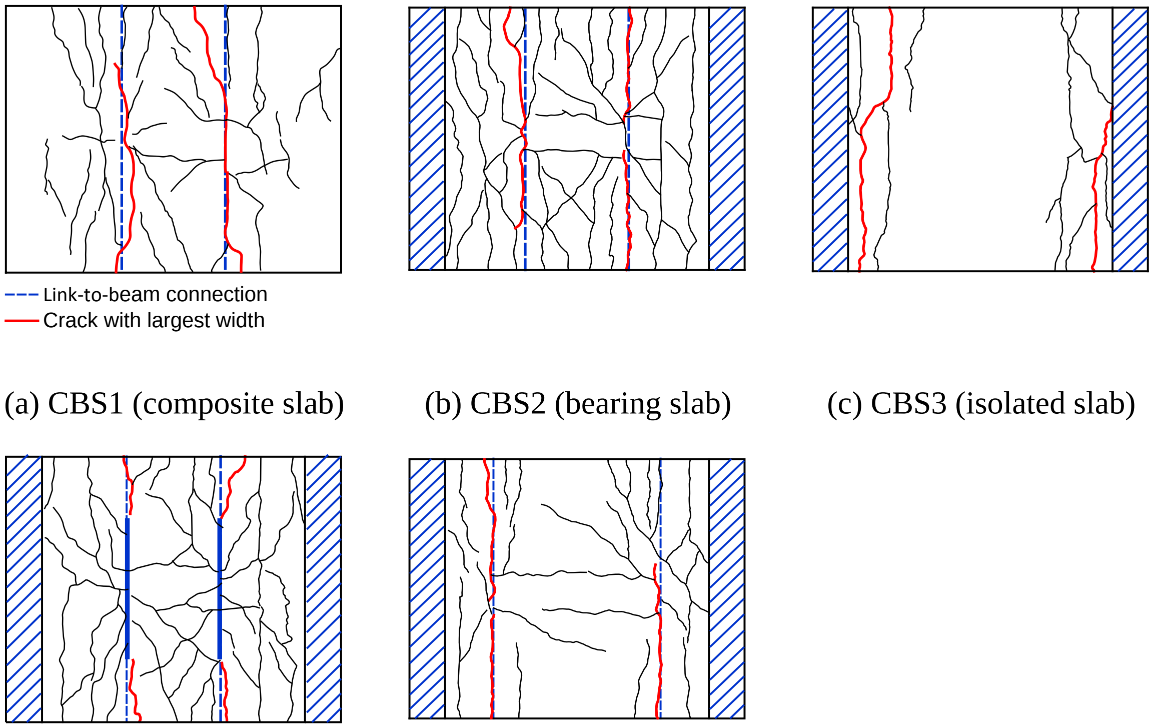

(a) CBS1 (composite slab) (b) CBS2 (bearing slab) (c) CBS3 (isolated slab)

(d) CBS4 (slotted slab) (e) CBS5 (bearing slab)

Fig. 10. Cracks developed in RC slabs

Finite element (FE) analysis was used to explain the observed cracking patterns of the RC slabs. Finite element models of Specimens CBS2 and CBS3 were developed using the FE program Abaqus 6.10 [17]. The steel beam, link and concrete slab were discretized using 8-node reduced integration (C3D8R) solid elements, and the rebars were represented by truss elements that were embedded into the slab concrete. The concrete was simulated by the damage plasticity model, where the axial compressive and tensile strength of the concrete was determined per the GB 50011-2010 code [12]. For simplicity, the materials of the steel beam segments and rebars were simulated by an elastic-perfectly plastic model that adopted the von Mises yield criterion. The shear links developed large overstrength due to cyclic hardening effect after shear yielding. To track this cyclic hardening effect, the Ramberg-Osgood model was used for the link steel in the FE simulation [18]. The parameters for Ramberg-Osgood model were determined from data regression of the cyclic coupon test data of steel plates. For the bearing slab, the interface between the top flange of beam segments and its above concrete was simulated using surface-to-surface contact interaction, where “hard” contact was assigned in the normal direction and Coulomb friction was assigned in the tangential direction. The beam segment end and the concrete slab end were rigidly connected to the end plate by “tie” constraint. The restraining plates that clamped the RC slab at the boundary (see. Figure 4) were also modeled, and they were rigidly connected to RC slab by “tie” constraint. The shear link was rigidly connected with the adjacent beam segments by “tie” constraint, neglecting the possible local deformation of the link-to-beam connection. More details of the FE model can be found in Wang 2016 [19].

The models were monotonically loaded to an inelastic beam rotation of 0.06 rad, equal to the beam rotation observed in the tests. Figure 11 illustrates the slab deformation of the bearing slab and isolated slab at beam rotation of 0.01 rad, depicting the contours of plastic strain (PE) distribution. The regions marked in grey are where the tensile plastic strain is larger than 0.03%. In the isolated slab, the large bending moment and associated plastic strains were produced only in the ends, while in the bearing slab, large bending moments and plastic strains was produced above the link-to-beam connection and at the ends. Bearing of the steel beam segment forced kinking deformation of RC slab, which resulted in longitudinal and diagonal cracks, in addition to transverse cracks.

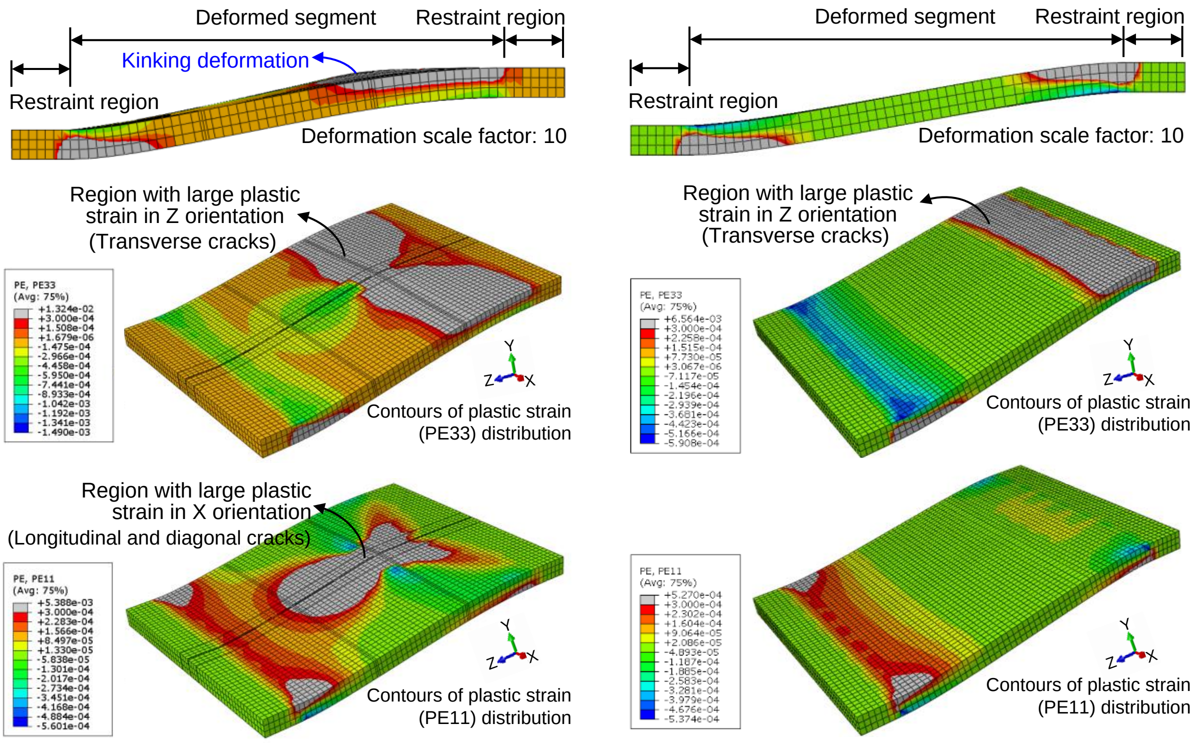

(a) Bearing slab (CBS2) (b) Isolated slab (CBS3)

Fig. 11. Deformation mode and plastic strain distribution of RC slabs

3.3.2. Crack width

Figure 10 indicates the locations of the widest cracks, which occurred at the slab ends for Specimen CBS3 and in the vicinity of link-to-beam connection for the other four specimens. Figure 12(a) shows the progression of maximum crack width for all specimens. The maximum crack width in the isolated slab and slotted slab was smaller than in the other slabs. Figure 12(b) shows the maximum width of residual crack in Specimen CBS2 through CBS5 measured at the instant when the coupling beams were unloaded to zero rotation. Similarly, the residual crack width in the isolated slab and slotted slab was smaller than in the other slab types. The Chinese Code for Design of Strengthening Concrete Structure (GB 50367-2010) [20] suggests repair methods for damaged slabs in relation to residual crack width. Cosmetic repair and injection of epoxy are recommended in this code. The applicable ranges of those repair methods are illustrated in Fig. 12(b).

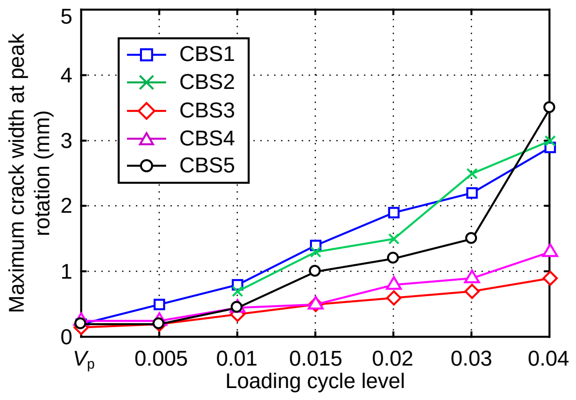

(a) Maximum crack width at peak rotation

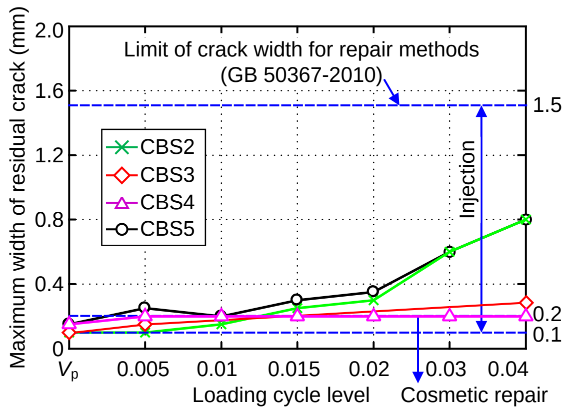

(b) Maximum width of residual crack

Fig. 12. Crack width of slabs at various loading levels

4. Effect of RC slabs on RSCBs

The bare steel specimens CB1 and CB2 reported by Ji et al. [4] are used for comparison. Specimen CB1 is identical to Specimens CBS1 through CBS4 in this study and Specimen CB2 is identical to CBS5, except for excluding the RC slabs. Figure 13 shows the examples for the comparison of hysteresis curves, CBS1 versus CB1, and CBS5 versus CB2. It is indicated that the addition of RC slabs increases the initial stiffness but otherwise has very limited influence on the hysteresis response.

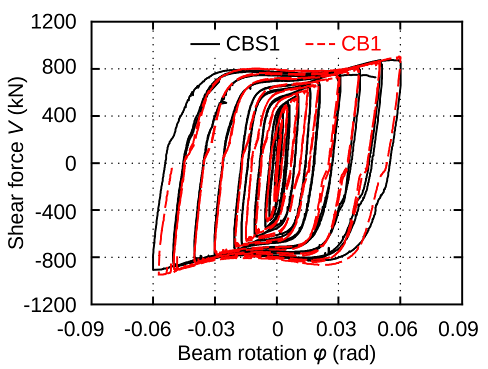

(a) CBS1 vs. CB1

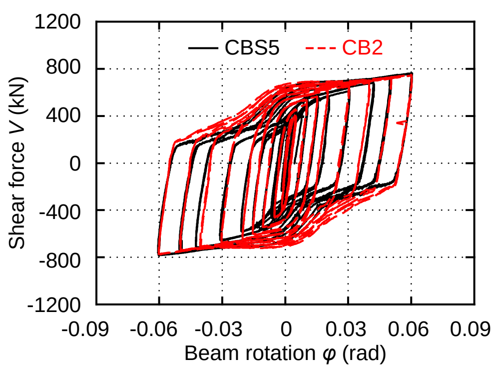

(a) CBS5 vs. CB2

Fig. 13. Comparison of hysteresis curves between bare RSCB and RSCB with RC slab

Table 4 summarizes the initial elastic stiffness, maximum shear strength and inelastic rotation capacity of the specimens, compared with the bare RSCBs. The initial elastic stiffness of each specimen is determined by the initial elastic response. Specimens CBS1, CBS2 and CBS4 had 30 to 40% larger initial elastic stiffness than the bare coupling beam counterpart CB1. Similarly, the initial stiffness was 19% greater for Specimen CBS5 than the bare coupling beam counterpart CB2. While Specimen CBS3 that had an isolated slab had a nearly identical stiffness with the bare coupling beam counterpart. However, as indicated in Fig. 13, at plastic stage, the presence of RC slabs had limited effect on the loading and unloading stiffnesses of the specimens. This is a result of loss of composite action after the bond between RC slab and steel beams was broken and damage to the RC slab during the cyclic loading.

Table 4. Comparison between bare RSCB and RSCB with RC slab

	Specimen No.	Elastic stiffness (kN/mm)		Maximum shear strength (kN)		Inelastic rotation capacity (rad)	
		Value	Normalized	Value	Normalized	Value	Normalized
RSCB with end plate connection	CB1	96.6	1.0	926	1.0	0.06	1.0
	CBS1	126.2	1.31	908	0.98	0.06	1.0
	CBS2	130.9	1.36	905	0.98	0.06	1.0
	CBS3	98.6	1.02	830	0.90	0.05	—
	CBS4	128.3	1.33	868	0.94	0.06	1.0
RSCB with splice plate connection	CB2	95.1	1.0	773	1.0	0.09	—
	CBS5	113	1.19	770	1.00	—	—

Table 4 also indicates that the presence of RC slabs had very limited influence on the maximum shear strength of RSCBs. The maximum shear strength of the specimens is defined as the maximum shear force measured prior to or at 0.06 rad beam rotation during which most specimens failed. Note that the strength of RC slabs was governed by their flexural strength of plastic hinges at their ends or at the regions above the link-to-beam connections (see Figure

11). The shear force of the RC slabs developed by this mechanism was estimated as 1% of the maximum shear strength of the links. Therefore, the RC slabs had limited contribution on the shear strength of RSCB specimens. Table 4 also indicates that, except for CBS3 which failed at 0.05 rad beam rotation due to weld defects, all specimens developed the same inelastic rotation capacity as their bare RSCB counterpart. The presence of RC slab appears to make no difference on the inelastic rotation capacity of RSBCs.

5. Development of fragility curves for RSCBs

In the next-generation seismic performance assessment of buildings (e.g., FEMA P-58 [21]), performance is expressed as the probable consequences in terms of direct economic losses, repair time and other metrics associated with a certain intensity of ground motion shaking. A fundamental component for performance assessment is reliable fragility functions, which are an estimate of damage in a structural component for a given engineering demand parameter.

FEMA P-58 [21] proposed fragility functions for EBF links using link rotation as the demand parameter and four unique damage states. FEMA P-58 also proposes repair methods for each damage state. Although the information for EBF shear links is directly applicable to RSCBs, the shear links in RSCBs generally have a smaller length ratio than EBF links because of the short span of coupling beams and the necessity to limit the link weight for replacement. Therefore, fragility curves for RSCBs are developed in the following using test data from this study and other recent experimental program on very short shear links [4,8].

Table 5 shows a summary of damage state descriptions and associated repair measures, as well as a visual illustration of the damage level for each damage state. DS0 corresponds to web yielding of the shear link. Repair of architectural enclosure in the vicinity of shear link is needed, while structural repair is not necessary because the shear strength and stiffness of the component are not affected. DS1 corresponds to damage to the slab above the RSCB, including cracks, spalling and crushing of concrete. Repair is required to ensure that the slab can serve as a rigid diagram for transmission of initial forces [14]. For the cracks less than 0.2 mm wide, GB 50367-2010 provision [20] recommends cosmetic repair to maintain first resistance and to prevent water infiltration. For cracks with width ranging from 0.1 mm to 1.5 mm, injection of epoxy is recommended as the repair method. However, this method is uneconomical if there are a large number of cracks. For severely damaged slabs with many wide cracks and/or concrete crushing, the portion of the slab above the RSCB might be replaced as suggested by Mansour et al. [14]. DS2 corresponds to local buckling of link web and flanges and global buckling of shear link. Heat strengthening could be used to straighten the buckled web and flanges, while link replacement is more appropriate if the buckling deformation is severe. DS3 corresponds to fracture of web and flange-to-end plate welds which lead to significant strength loss of the link, in which case link replacement shall be necessary.

Table 5. Damage states and repair methods of RSCBs

ID	Damage state	Repair methods	Photographs for each damage state
DS0	· Shear yielding of link web	· Repair of architectural enclosure	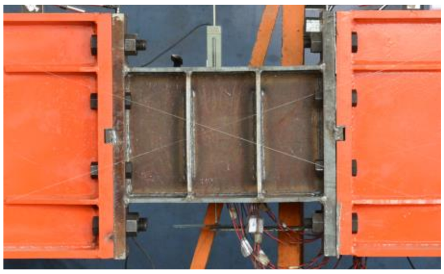
DS1	· Substantial slab damage	· Cosmetic repair · Injection of epoxy · Replacement of the local slab above the RSCB.	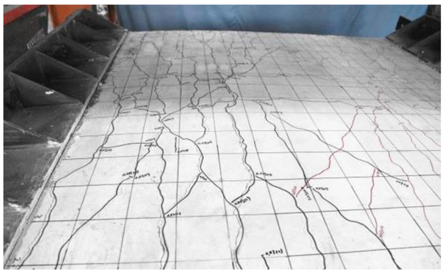

DS2	· Link web buckling · Link flange buckling · Link global buckling	· Heat strengthening · Replacement of shear link	
DS3	· Link web fracture · Link flange-to-end plate weld fracture	· Replacement of shear link	

Table 6 summarizes the test data of the link rotation corresponding to various damage states. Note that the link rotation is used as the demand parameter for the fragility curves, as most damage of RSCBs is concentrated in the shear links. The fragility curves for the three damage states DS1, DS2 and DS3, shown in Fig. 14, were obtained by fitting a lognormal distribution to the test data using maximum likelihood method. This method finds the parameters such that the resulting distribution has the highest likelihood of having produced the observed data [21]. It should be noted that DS1, which is associated with the repair method of necessary concrete replacement, was established based on Specimens CBS2, CBS3 and CBS5 only. Specimen CBS1 with a composite slab is not included because the test results suggest against the use of composite slabs in RSCBs. The test results indicate that the slotted slab has similar cracking pattern and local concrete crushing as the bearing slab, although the maximum crack width is smaller than the bearing slab. The slotted slab does not show significant advantages than the bearing slab in terms of post-quake repair, while the former needs additional construction effort and it might influence the rigid diagram of slab system. As such, the use of slotted slabs is not recommended either and Specimen CBS4 with a slotted slab is not included for establishing the fragility curve of DS1. Compared to the bearing slab, the isolated slab can accommodate larger link rotation before reaching DS1. The median link rotation for DS1, 0.05 rad, is slightly larger than the value for EBF links suggested by FEMA P-58. The median link rotations for DS2 and DS3, 0.09 and 0.11 rad, respectively, are larger than the values of 0.06 and 0.08 rad for EBF links suggested by FEMA P-58, as the very short links used in RSCBs can develop larger inelastic rotation than the EBF links [8]. The dispersions of link rotation of DS2 and DS3 are 0.19 and 0.15 respectively, and that value is larger for DS1, reaching 0.30.

Table 6. Link rotation corresponding to various damage states

Test	Spec. No.	Link rotation corresponding to damage state (rad)		
		DS1	DS2	DS3
Shear link test [8]	L11C	—	0.10	0.12
	L11	—	0.11	0.13
	L12	—	0.08	0.09
	L13	—	0.07	0.13
	L21	—	0.11	0.11
	L22	—	0.13	0.13
	Q11	—	0.09	0.11
	Q12	—	0.09	0.11
	Q13	—	0.07	0.11
	Q21	—	0.11	0.09
	Q22	—	0.09	0.09
Replaceable steel coupling beam test [4]	CB1	—	0.11	0.11
	CB2	—	0.13	0.13
	CB3	—	0.10	0.12
This test	CBS1	—	0.12	0.12
	CBS2	0.03	—	0.12
	CBS3	0.08	0.12	0.12
	CBS4	—	—	0.13
	CBS5	0.04	—	—

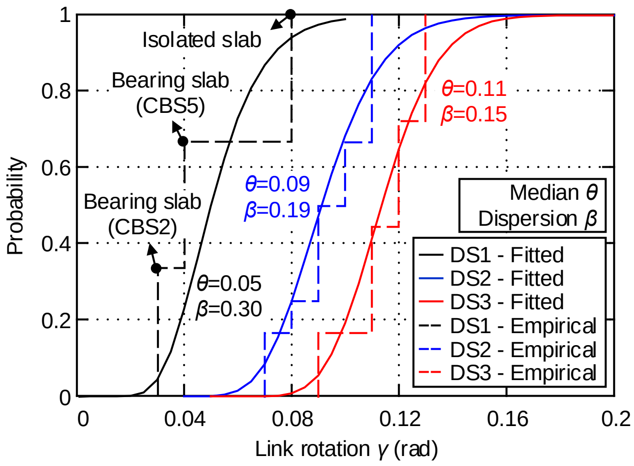

Fig. 14. Fragility curves of each damage state

6. Conclusions

This paper presents a series of cyclic loading tests performed to investigate the cyclic behavior of RSCBs with RC slabs and to identify reasonable slab configuration that minimizes the damage to RC slabs. Four different slab types were examined. Fragility curves of RSCBs were developed based on test data from this study and past programs. Major findings from the study are summarized as follows:

(1) The composite slab sustained very severe damage, as a result of pulling out of shear studs followed by punching failure of the slab. Use of shear connections is thus not recommended between the RSCBs and RC slabs.

(2) Among the four slab types examined, the isolated slab which avoided contact between the RC slab and RCSB, showed the least damage, and hence allows the easiest repair.

(3) The RC slabs had limited effect on the shear strength and inelastic rotation capacity of RSCBs. Some types of slabs increased the initial elastic stiffness of RSCBs, but in the plastic stage, none of the slabs affected the loading or unloading stiffness.

(4) Based on the test observations, four damage states and repair methods for RSCBs similar to those suggested for EBF links by FEMA P-58 are proposed. The fragility curve for DS1

through DS3 of RSCBs has larger median link rotation than the suggested value for EBF links, as the links used in RSCBs are usually shorter than the EBF links.

Acknowledgements

The work presented in this paper was sponsored by the International Science & Technology Cooperation Program of China (Grant No. 2014DFA70950) and National Natural Science Foundation of China (Grants No. 51261120377). The writers wish to express their sincere gratitude to the sponsors.

References

[1] Fortney PJ, Shahrooz BM, Rassati GA. Large-scale testing of a replaceable steel coupling beam. Journal of Structural Engineering (ASCE) 2007, 133(12): 1801-1807.

[2] Christopoulos C, Montgomery MS. Viscoelastic coupling dampers (VCDs) for enhanced wind and seismic performance of high-rise buildings. Earthquake Engineering and Structural Dynamics 2013, 42(15): 2217-2233.

[3] Lu X, Chen Y, Jiang H. Research progress in new replaceable coupling beams. Journal of Earthquake Engineering and Engineering Vibration 2013, 33(1): 8-15 (in Chinese).

[4] Ji X, Wang Y, Ma, Q, Okazaki T. Cyclic behavior of replaceable steel coupling beams. Journal of Structural Engineering (ASCE) 2017, 143(2): 04016169.

[5] Ji X, Liu D, Sun Y, Molina Hutt C. Seismic performance assessment of a hybrid coupled wall system with replaceable steel coupling beams versus traditional RC coupling beams. Earthquake Engineering and Structural Dynamics, 2017, 46(4): 517-535.

[6] Kasai K, Popov EP. General behavior of WF steel shear link beams. Journal of Structural Engineering 1986, 112(2): 362-382.

[7] Dusicka P, Itani AM, Buckle IG. Cyclic behavior of shear links of various grades of plate

steel. Journal of Structural Engineering 2010, 136(4): 370-378.

[8] Ji X, Wang Y, Ma Q, Okazaki T. Cyclic behavior of very short steel shear links. Journal of Structural Engineering (ASCE) 2016, 142(2): 04015114.

[9] AISC. Seismic Provisions for Structural Steel Buildings (ANSI/AISC 341-10). American Institute of Steel Construction: Chicago, 2010.

[10] Okazaki T, Arce G, Ryu HC, Engelhardt MD. Experimental study of local buckling, overstrength, and fracture of links in eccentrically braced frames. Journal of Structural Engineering (ASCE) 2005, 131(10): 1526-1535.

[11] Okazaki T, Engelhardt MD. Cyclic loading behavior of EBF links constructed of ASTM A992 steel. Journal of Constructional Steel Research 2007, 63(6): 751-765.

[12] CMC. Code for Design of Concrete Structures (GB 50010-2010). China Ministry of Construction: Beijing, 2010 (in Chinese).

[13] Ricles JM, Popov EP. Composite action in eccentrically braced frames. Journal of Structural Engineering (ASCE) 1989, 115(8): 2046-2066.

[14] Mansour N, Christopoulos C, Tremblay R. Experimental validation of replaceable shear links for eccentrically braced steel frames. Journal of Structural Engineering (ASCE) 2011, 137(10): 1141-1152.

[15] Castiglioni CA, Kanyilmaz A, Calado L. Experimental analysis of seismic resistant composite steel frames with dissipative devices. Journal of Constructional Steel Research 2012, 76: 1-12.

[16] McDaniel CC, Uang CM, Seible F. Cyclic testing of built-up steel shear links for the new Bay Bridge. Journal of Structural Engineering (ASCE) 2003, 129(6): 801-809.

[17] ABAQUS. Analysis User's Manual. Version 6.10. USA: ABAQUS Inc., Dassault

Systèmes, 2010.

[18] Dusicka P, Itani AM, Buckle IG. Cyclic response of plate steels under large inelastic strains. Journal of Constructional Steel Research 2007, 63: 156-164.

[19] Wang Y. Study on seismic behavior and design of replaceable steel coupling beams with RC slabs. Master’s thesis, Beijing: Tsinghua University, 2016 (in Chinese).

[20] CMC. Code for Design of Strengthening Concrete Structure (GB 50367-2010). China Ministry of Construction: Beijing, 2010 (in Chinese).

[21] ATC. FEMA P-58-1: Seismic Performance Assessment of Buildings. Volume 1 – Methodology. Federal Emergency Management Agency: Washington, DC, 2012.